PCCP

Accepted Manuscript

ROYAL SOCIETY OF CHEMISTRY

www.rsc.org/pccp

Journal Name

RSCPublishing

ARTICLE

In situ fabrication of Ag_3PO_4/TiO_2 nanotube heterojunction with enhanced visible−light photocatalytic activity

Cite this: DOI: 10.1039/x0xx00000x

Received 00th January 2012,
Accepted 00th January 2012

DOI: 10.1039/x0xx00000x

www.rsc.org/

Zhen Wei Tong,[ad] Dong Yang,[bcd] Yuan Yuan Sun,[bd] Yao Tian[b] and Zhong Yi Jiang*[ad]

Ag_3PO_4/TiO_2 nanotube (TNT) heterojunction was firstly fabricated *via* a facile *in situ* growth method. Hemispherical Ag_3PO_4 nanocrystals are uniformly grown on the TNT surface, and their size is confined to 5−10 nm. A joint area is observed distinctly between Ag_3PO_4 nanocrystal and TNT, indicating the formation of Ag_3PO_4/TNT heterojunction. Compared with pure Ag_3PO_4, the Ag_3PO_4/TNT heterojunction possesses more active sites, less bulk defects, and more efficient electron−hole separation, as well as higher dye adsorption, thus exhibiting significantly elevated photocatalytic activity in the Rhodamine B (RhB) degradation. The study of reactive species demonstrates that the photocatalytic degradation of RhB over Ag_3PO_4/TNT heterojunction is primarily driven together by photogenerated h^+ and ·OH radicals. This easily−fabricated Ag_3PO_4/TNT heterojunction, with promising photocatalytic activity, may find potential applications in energy and environmental related areas.

Introduction

Ag_3PO_4 semiconductor has been reported as a novel visible light driven photocatalyst for the environment decontamination and oxygen evolution from water splitting, with quantum efficiency up to 90% at wavelength around 420 nm. [1–2] The photocatalytic activity of Ag_3PO_4 is dramatically higher than that of common visible−light photocatalysts, such as N−doped TiO_2, $BiVO_4$ and g−C_3N_4. [2–3] Unfortunately, the Ag_3PO_4 photocatalyst is photochemically unstable, since silver salts are prone to decompose under light irradiation, which restricts its performance. [4] Thus, a strategy *via* combining Ag_3PO_4 with carbon materials [4–5] or stable semiconductors, such as silver halide, TiO_2, g−C_3N_4, Cr−$SrTiO_3$, and MoS_2, [3, 6–9] has been employed to improve the photocatalytic stability and activity. However, the carbon materials generally possess a more negative conduction−band potential than that of Ag_3PO_4, which prevents the transfer of photo−generated electrons from Ag_3PO_4 to them. The silver halides usually possess the limited adsorption of organic pollutants due to its low surface area and weak electrostatic interaction with organic molecules. In contrast, the metallic silver (Ag^0) nanoparticles deposited on Ag_3PO_4 crystals to form multiple heterostructrue showed desirable recycling stability. [10–11] However, it is still elusive how to stabilize the Ag_3PO_4 particles with controlled morphology and dispersibility. In addition, the Ag/Ag_3PO_4 composite photocatalyst also suffers from high cost, hindering its broad applications in the photocatalytic processes. [8, 12] Therefore, it is a challenging task to develop a facile and economical method to fabricate the high−efficiency and stable Ag_3PO_4 heterojunction with other semiconductor.

Compared with commonly used nanoparticles or bulk materials, TiO_2 nanotubes (TNT), as one−dimension (1D) supports, can afford unique benefits as photocatalyst in view of the following features. [13–15] First, the 1D geometry facilitates fast and tunable charge transport and decouples the direction of charge carrier collection. Second, the nanotubular structure is expected to have a high surface−to−volume ratio and well confine with the attached particles. Third, it can be easily recycled from a solution by sedimentation. Up to now, the potential applications of TNT−based materials have been reported in diverse fields, such as dye−sensitized solar cell, [16] photocatalysis, [17–18] and drug delivery. [19] Therefore, it should be of significant interest to investigate the preparation and potential application of Ag_3PO_4/TNT nanocomposites as photocatalysts. Chen and co−workers [7] fabricated a novel heterostructure of Ag/Ag_3PO_4/TiO_2 photoelectrode by covering the surface of TiO_2 nanotube arrays with Ag_3PO_4 through the chemical bath deposition process and UV irradiation, which showed high photocatalytic activity for the removal of 2−chlorophenol due to effective separation of photo−generated electron−hole pairs and large quantity of dye adsorption. Niraula *et al.* [20] reported a Ag_3PO_4/TiO_2 nanotube arrays composite with enhanced photocatalytic degradation performance, since it possesses fast charge carrier mobility and separation. However, the synthetic procedure of these composites is tedious and difficult to scale up (ten repetition of immersing). [7, 20] Moreover, the morphology and distribution of Ag_3PO_4 particles on the surface of arrays, as well as the recycling stability of Ag_3PO_4 particles, still need to be improved. Until now, there are only these two literatures involving Ag_3PO_4 deposition on the TiO_2 nanotube arrays, and no study on the Ag_3PO_4/TNTs heterojunction has been published.

Herein, a novel kind of Ag_3PO_4/TNT heterojunction was firstly fabricated *via* the *in situ* deposition of Ag_3PO_4 nanoparticles on the TNT surface. The motivation of fabricating Ag_3PO_4/TiO_2 nanotube heterojunction can be analyzed from the following two aspects: one is to facilitate the separation of photo−generated carriers in Ag_3PO_4 *via* the band match between Ag_3PO_4 and TNT, thus improving the photocatalytic activity; the other is to optimize the structure and performance of Ag_3PO_4 by using TNT as the support. The morphology and structure of the Ag_3PO_4/TNT heterojunction were characterized. Furthermore, the visible−light photocatalytic activity and stability, as well as the photocatalytic mechanism of the Ag_3PO_4/TNT heterojunction for decomposing Rhodamine B (RhB) were investigated.

Experimental

Fabrication of TiO_2 nanotube

Rutile titanium dioxide powders (Sigma−Aldrich), silver nitrate, disodium hydrogen phosphate (Tianjin Guangfu Co.) and sodium hydroxide were used as received and without any further purification.

Regular titanate nanotubes were prepared by a hydrothermal method reported by Geng *et al*. [21] Typically, nano−sized rutile titanium dioxide powders (2 g) were firstly dispersed in a NaOH solution (85 mL, 10 mol L^{-1}) under magnetic stirring. Then, the suspension was put into a sealed Telfon−lined vessel (100 mL) and statically heated at 130 ^oC for 72 h. After centrifugation and washing with deionized water, a white precipitate was obtained. Subsequently, the precipitate was immersed in a HCl solution (100 mL, 0.1 mol L^{-1}) for 10 h, followed by washing with deionized water until pH 7.0. After dried at 60 ^oC for 12 h, titanate nanotubes were acquired finally. To prepare anatase TNT, titanate nanotubes were further calcined at 380 ^oC for 1 h.

Fabrication of Ag_3PO_4/TNT heterojunction

Ag_3PO_4 nanoparticles were deposited onto the as−prepared crystallized TNT surface *via* an *in situ* precipitation process, as shown in Scheme 1. In a typical process, 50 mg of TNT was first dispersed in 10 mL of deionized water, and sonicated for 1 h with 100 Hz frequency. Subsequently, 10 mL of $AgNO_3$ solution with a certain concentration was added to the TNT suspension (pH=7) under magnetic stirring, keeping for 12 h in the dark. The previously dissolved 1 mol L^{-1} of Na_2HPO_4 was added dropwise to the suspension, and the mole ratio of Na_2HPO_4 to $AgNO_3$ was made to be 1: 3. The resulting suspension was magnetically stirred for 5 h in the dark, during which its color changed to yellow. The deposit was then filtered, washed and dried for the photocatalytic reaction and characterization. The composite samples were marked as Ag_3PO_4/TNT−10, Ag_3PO_4/TNT−15, Ag_3PO_4/TNT−20, Ag_3PO_4/TNT−40, Ag_3PO_4/TNT−60, Ag_3PO_4/TNT−80 according to the final concentration of $AgNO_3$ (10, 15, 20, 40, 60 and 80 mmol L^{-1}) in the reaction solution, respectively. For comparison, Ag_3PO_4 particles were also prepared under the same conditions without TNT.

Characterization

The transmission electron microscopy (TEM) and high−resolution transmission electron microscopy (HRTEM) imaging were performed on a Tecnai G2 F20 transmission electron microscope at an accelerating voltage of 200 kV. The crystal phase was obtained by X−ray diffraction (XRD) patterns with a Rigaku D/max 2500V/PC X−ray diffractometer (Cu Kα, λ=0.154 nm, 40 kV, 200 mA). Scattered radiation was detected in the angular range of 5−80º with a scan rate of 4º min^{-1}. The Fourier transform infrared (FTIR) spectra were recorded in transmission mode from 400 to 4000 cm^{-1} on a FTIR spectrometer using KBr discs. Chemical compositions of the samples were analyzed on a Perkin−Elmer PHI 1600 ESCA X−ray photoelectron spectroscope (XPS) with a monochromatic Mg Kα radiation (1253.6 eV), and the binding energies were normalized to C 1s peak at 284.6 eV. The light absorption properties were measured using a UV−vis diffuse reflectance spectrophotometer (Hitachi, U−3010) with a wave−length range of 200−800 nm, and $BaSO_4$ was used as a reference. UV−vis spectra were obtained on a Hitachi U−3100 spectrophotometer.

Photocatalytic activity

Rhodamine B, a widely used dye, was chosen as a model pollutant to examine the visible−light photocatalysis of as−prepared Ag_3PO_4/TNT samples. In a typical photocatalytic experiment, 50 mg photocatalyst powders were dispersed in 50 mL of 10 mg mL^{-1} RhB solution at room temperature under visible−light irradiation. The light source was a 500 W Xe lamp (Shanghai−BiLang Company, BLV−GHX−V) equipped with a UV cutoff filter (λ>420 nm). Prior to irradiation, the RhB solution containing photocatalyst was stirred in the dark for 60 min to ensure that the photocatalyst surface was saturated with dye molecules. The RhB degradation was monitored by measuring the changes of UV−vis absorption spectra as a function of irradiation time. The photocatalytic activity of TNT and Ag_3PO_4 were also determined under the same conditions as the control.

For an in−depth understanding for the role of photogenerated radical species in the photocatalytic degradation of RhB, a series of controlled experiments were further performed. Three radical scavengers including disodium ethylenediaminetetraacetate (EDTA, 10 mmol L^{-1}), benzoquinone (1 mmol L^{-1}) and methanol (1: 15/v:v), were added into the reaction system to investigate the specific reactive species involved in the photocatalytic degradation of RhB over Ag_3PO_4/TNT photocatalysts, respectively. Furthermore, the changes of UV−vis absorption spectra of RhB over Ag_3PO_4/TNT photocatalysts were tested to confirm the RhB degradation pathway.

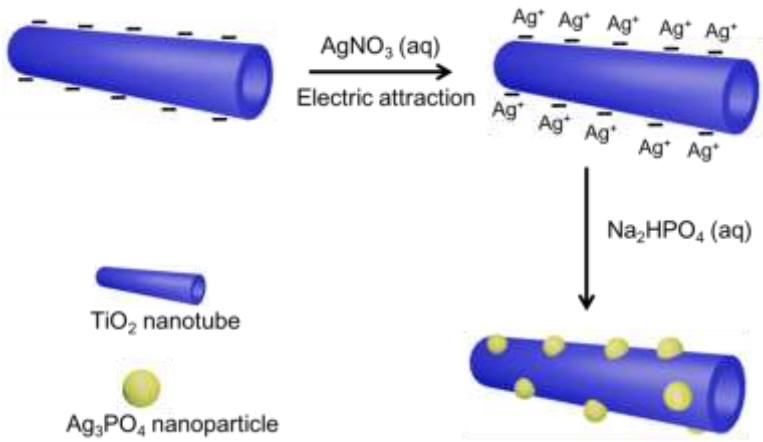

Scheme 1 Schematic synthetic procedure of Ag_3PO_4/TNT heterojunction.

Results and discussion

Morphology and structure of Ag_3PO_4/ TNT

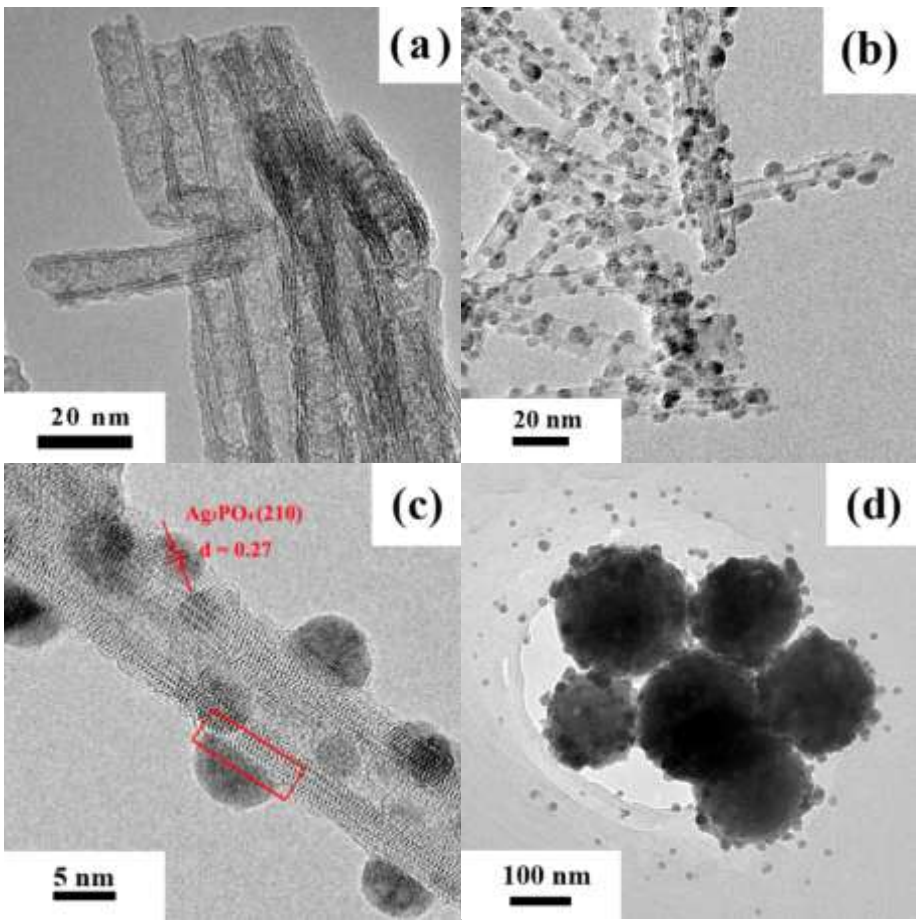

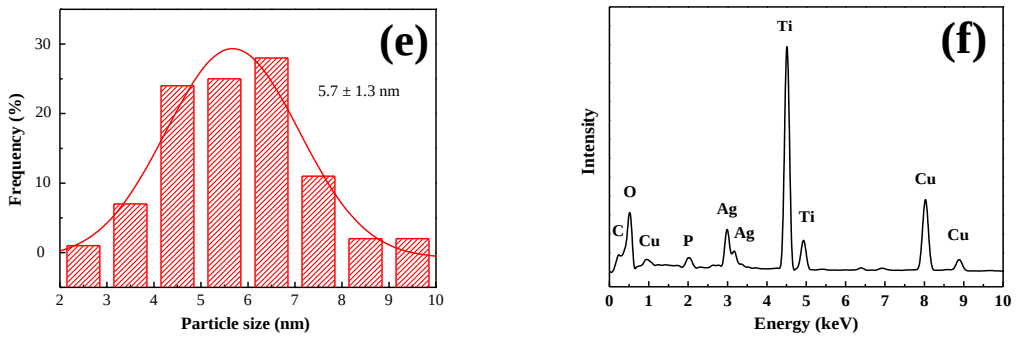

Fig. 1 TEM images of TNT (a), Ag_3PO_4/TNT−10 (b), and Ag_3PO_4 (d); HRTEM image (c), Ag_3PO_4 particle−size histogram (e) and EDX spectrum (f) of Ag_3PO_4/TNT−10.

The morphology of as−prepared Ag_3PO_4/TNT samples was characterized using TEM and HRTEM, and shown in Fig. 1. The pure TNT exhibits a typical nanotubular structure with the outer diameter and the inner diameter of approximately 10 and 5 nm, respectively (Fig. 1a). In the Ag_3PO_4/TNT−10 sample (Fig. 1b), many nanoparticles about 5.7±1.3 nm in size (Fig. 1e) are uniformly loaded on the TNT surface; whereas the prepared Ag_3PO_4 particles without TNT become 150−250 nm in size (Fig 1d). The HRTEM image of Ag_3PO_4/TNT (Fig. 1c) demonstrates clearly that these nanoparticles are hemispherical, which bind tightly on the TNT surface. Simultaneously, their lattice spacing is observed to be about 0.27 nm, which corresponds to the (210) plane of Ag_3PO_4, [22] confirming that these nanoparticles are Ag_3PO_4 crystals. It is inferred that the TNT plays an important role during the *in situ* growth of Ag_3PO_4 particles on the TNT surface. The Ag^+ ions are firstly adsorbed on the negatively−charged TNT surface *via* the electrostatic interaction, and then the nucleation and growth of Ag_3PO_4 occur on the TNT surface as PO_4^{3-} is added in the reaction (Scheme 1). Due to the surface confinement of TNT, [13] the growth and aggregation of Ag_3PO_4 are inhibited, thus leading to the formation of uniform Ag_3PO_4 nanoparticles. In addition, TNT exhibits distinct lattices, indicating that it is well−crystallized after calcination at 380 ^oC for 1 h. It is noteworthy that Ag_3PO_4 nanoparticles are well connected with TNT *via* the lattice fuse (the red box in Fig. 1c), which is advantageous for the charge transfer between Ag_3PO_4 and TNT. No bare TNT or peeled−off Ag_3PO_4 nanoparticle was observed, even though the Ag_3PO_4/TNT sample was treated ultrasonically for 1 h prior to the TEM characterization. Herein, it is speculated that Ag_3PO_4 nanoparticles form the covalent bond with TNT after the *in situ* growth process, rather than the weak physical interaction. In order to further confirm the composition, the Ag_3PO_4/TNT sample was also investigated by the EDX spectrum (Fig. 1f). It is observed that this sample is composed of O, Ag, P and Ti elements, eliminating the impurity elements of C and Cu from the testing instrument. Furthermore, the corresponding EDX elemental mapping (Fig. 2) reveals that the Ti and O elements mostly exist at the inner part of nanocomposite, while the Ag and P elements mainly distribute at the nanocomposite surface. Notably, the Ag mapping is basically coincided with the P mapping, confirming the existence of Ag_3PO_4 in the nanocomposite.

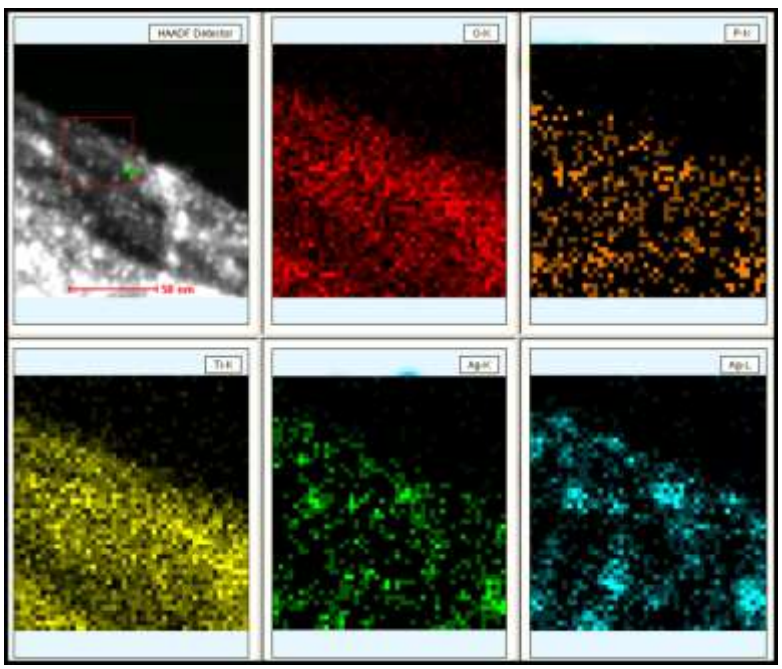

Fig. 2 Scanning TEM−energy dispersive X−ray spectroscope (STEM−EDX) elemental mapping results of Ag_3PO_4/TNT−20.

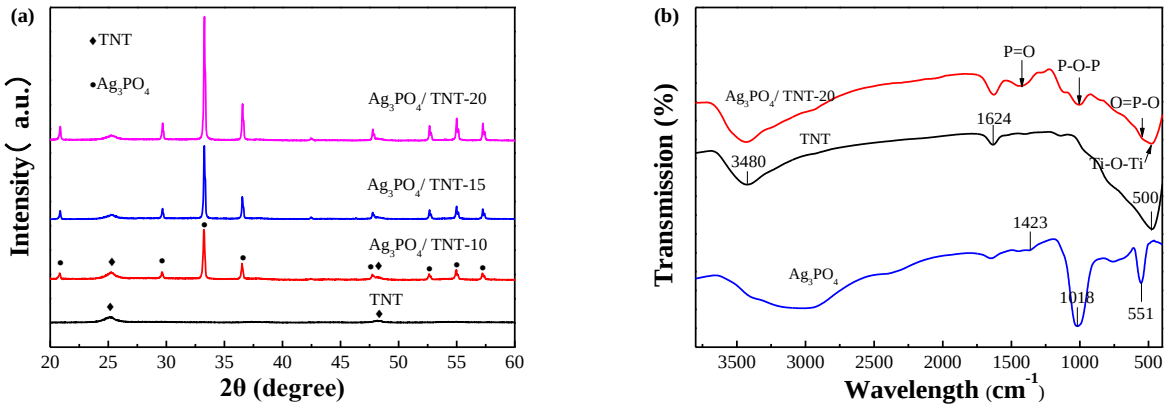

Fig. 3 (a) XRD patterns of TNT and Ag_3PO_4/TNT with different Ag_3PO_4 loadings; (b) FT−IR spectra of TNT, Ag_3PO_4 and Ag_3PO_4/TNT−20.

X−ray diffraction (XRD) and Fourier transform infrared (FTIR) spectra of as−prepared Ag_3PO_4/TNT heterojunctions were recorded to further confirm their composition and crystalline structure. In the XRD curve of TNT (Fig. 3a), the characteristic peaks at 2θ values of 25.3° and 48.1° are readily indexed as the anatase phase (JCPDS 21−1272). [23] Besides the peaks of anatase crystal, the curves of three Ag_3PO_4/TNT samples demonstrate the diffraction peaks at 2θ values of 20.9°, 29.7°, 33.3°, 36.6°, 47.8°, 52.7°, and 55.0 °, which are ascribed to the (110), (200), (210), (211), (310), (222) and (320) crystal planes of Ag_3PO_4 (JCPDS 06−0505), respectively. [24] No impurity peak of metal Ag and other silver salts appears in the XRD pattern of Ag_3PO_4/TNT, indicating that Ag_3PO_4 prepared by this method is pure. [7] Moreover, the intensity of Ag_3PO_4 peaks is high, suggesting their high degree of crystallinity. On the basis of the full width at half−maximum (fwhm) of the (210) diffraction peak of Ag_3PO_4, the crystallized sizes of Ag_3PO_4 in Ag_3PO_4/TNT−10, Ag_3PO_4/TNT−15 and Ag_3PO_4/TNT−20 are calculated to be about 5.6, 6.5 and 8.4 nm by the Debye−Scherrer formula, respectively. This result reveals that the size of Ag_3PO_4 nanocrystals in Ag_3PO_4/TNT heterojunction can be regulated easily by changing the initial $AgNO_3$ concentration. [12] As shown in Fig. 3b, three peaks at 551, 1018 and 1423 cm^{-1} in the FTIR spectrum of Ag_3PO_4 are attributed to the O=P−O flexural vibration, the asymmetric vibration of P−O and P=O in Ag_3PO_4, respectively; [25] while three characteristic peaks located at about 500, 1624 and 3480 cm^{-1} in the FTIR spectrum of TNT are ascribed to the vibration of Ti−O−Ti, the water molecule adsorbed on the surface and the external −OH group on the TNT surface, respectively. [26] Although no new peak appears in the FTIR spectrum of Ag_3PO_4/TNT, the peak of P−O asymmetric vibration shifts from 1018 to 1008 cm^{-1}, indicating the strong interaction between Ag_3PO_4 and TNT.

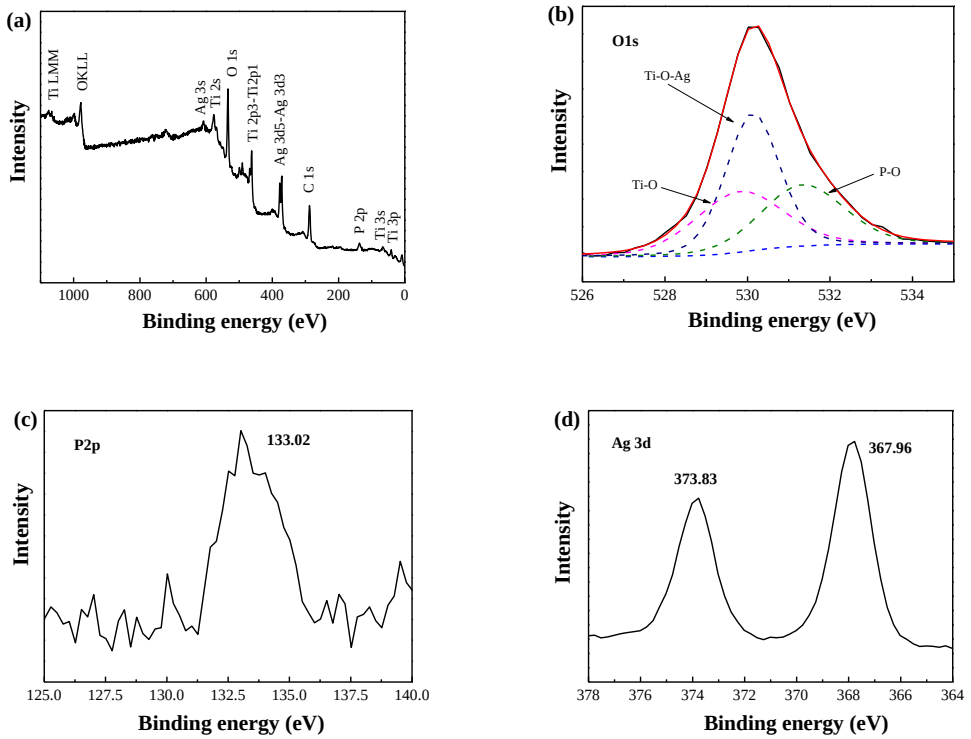

Fig. 4 XPS spectra of Ag_3PO_4/TNT−20: (a) survey spectrum, (b) O 1s, (c) P 2p, and (d) Ag 3d.

XPS was carried out to further determine the element composition of as−prepared Ag_3PO_4/TNT heterojunctions and analyze the chemical status of relevant elements. Fig. 4a illustrates the full XPS spectrum of Ag_3PO_4/TNT heterojunction, revealing the presence of Ti, O, Ag, P and C elements. The high−resolution O 1s XPS curve can be fitted into three peaks at 529.8, 530.1 and 531.3 eV by using Gaussian−Lorentzian peak fitting (Fig. 4b), which are assigned to the Ti−O, Ti−O−Ag [27] and P−O bond, [25] respectively. The presence of Ti−O−Ag bond indicates that a strong covalent interaction exists between Ag_3PO_4 and TNT, confirming the formation of the heterojunction structure, which is critical for the electron−hole separation. In Fig. 4c, the P 2p peak of Ag_3PO_4/TNT appears at 133.0 eV, which corresponds to P^{5+} of PO_4^{3-} ions according to the previous report. [11] The Ag 3d spectrum (Fig. 4d) exhibits two peaks at 368.0 (Ag3d5/2) and 373.8 eV (Ag3d3/2), originating from the Ag^+ ions in Ag_3PO_4. [2] No other peak is shown in the Ag 3d region after Gaussian curve fitting, indicating the only existence of Ag^+ ions in the sample.[7, 11]

Optical absorption properties of Ag_3PO_4/TNT

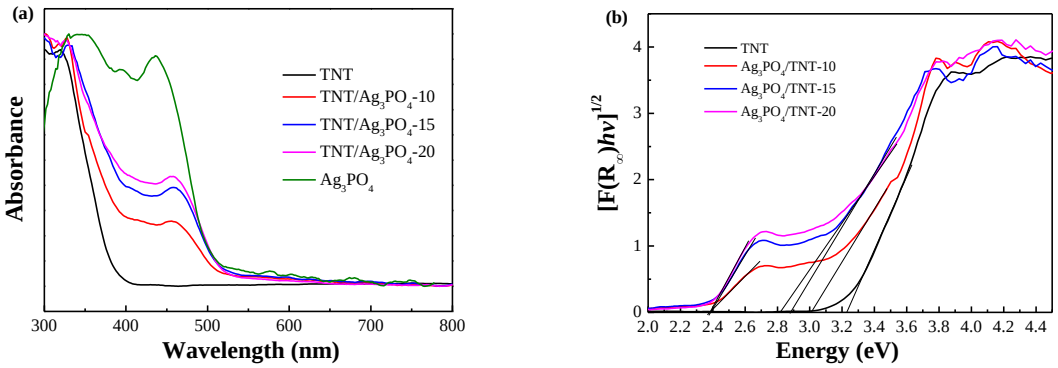

Fig. 5 (a) DRS spectra of TNT, Ag_3PO_4 and Ag_3PO_4/TNT with different Ag_3PO_4 loadings and (b) their corresponding plots of $[F(R_\infty)hv]^{1/2}$ versus hv.

UV−vis diffuse reflectance spectra (DRS) of pure TNT, Ag_3PO_4 and Ag_3PO_4/TNT with different Ag_3PO_4 loadings are displayed in Fig. 5a. It can be seen that pure Ag_3PO_4 sample can absorb both UV and visible light with an absorption edge about 530 nm, corresponding to a band gap energy of 2.45 eV, which agrees with the light−absorption property of Ag_3PO_4 powders reported by literatures. [3, 8] All Ag_3PO_4/TNT samples exhibit strong visible−light absorption, confirming clearly that the Ag_3PO_4 modification can affect the optical property of TNT. Furthermore, with increasing the Ag_3PO_4 mass ratio, the absorption intensity of Ag_3PO_4/TNT photocatalysts obviously increases in the visible region. Notably, two absorption edges are observed in the curve of Ag_3PO_4/TNT, *e.g.* Ag_3PO_4/TNT−20 at 450 nm and 530 nm, which are assigned to the absorption edges of TNT and Ag_3PO_4, respectively. Compared to that of pure TNT, the absorption edge of TNT in the Ag_3PO_4/TNT−20 heterojunction has an obviously red shift of about 50 nm, which can be attributed to the heteroepitaxial growth of Ag_3PO_4 on the TNT surface. [28] This result is accordance with the report of AgX/Ag_3PO_4 heterojunction in literature. [28] The band gap energy (E_g) of the resulting Ag_3PO_4/TNT samples can be estimated from a plot of $[F(R_\infty)hv]^{1/2}$ versus hv, [29] where R is the reflectance coefficient, h is the Planck's constant and v represents the light frequency. The tangent interception to the X axis would give a good approximation of E_g of Ag_3PO_4/TNT samples (Fig. 5b). The band gaps of Ag_3PO_4/TNT samples originated from Ag_3PO_4 part are almost the same (2.40 eV); while those of Ag_3PO_4/TNT−10, Ag_3PO_4/TNT−15 and Ag_3PO_4/TNT−20 originated from TNT part are 3.01, 2.90 and 2.81 eV, respectively. The Ag_3PO_4/TNT heterojunction with narrow bandgap should have high photocatalytic activity for target reactions.

Photocatalytic Activity

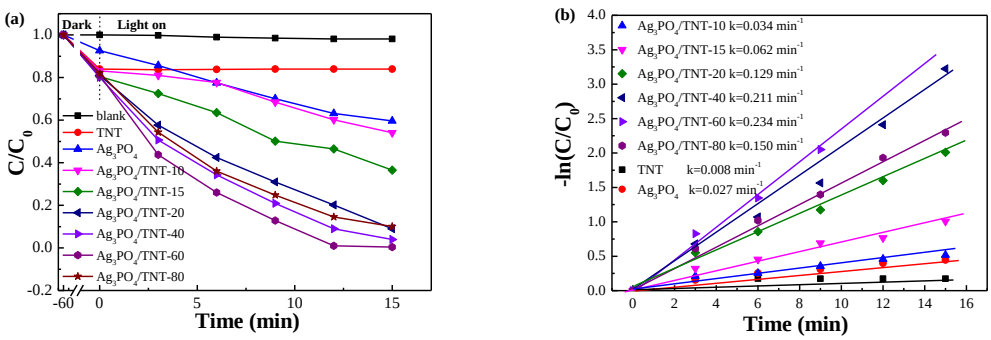

Fig. 6 Photocatalytic degradation curves of RhB over TNT, Ag_3PO_4 and Ag_3PO_4/TNT (a) with different Ag_3PO_4 loadings under visible light, and (b) their corresponding kinetic simulation curves.

Photocatalytic activities of TNT, Ag_3PO_4 and Ag_3PO_4/TNT photocatalysts were carried out for decomposing RhB under visible−light irradiation (λ>420 nm), and the results are shown in Fig. 6a. In the absence of photocatalyst, the RhB concentration remains almost unchanged within 15 min under visible light irradiation, indicating that RhB is hardly self−degradable under this condition. Pure TNT doesn't almost degrade the RhB within 15 min, even though it appears high adsorption capability for RhB. All Ag_3PO_4/TNT samples exhibit higher photocatalytic activity than pure Ag_3PO_4, and the Ag_3PO_4/TNT−60 sample exhibits the best photocatalytic activity, which can decompose 99.6% RhB within 12 min under visible light irradiation. Since the $AgNO_3$ concentration is lower than 60 mmol L^{-1}, the photocatalytic activity of Ag_3PO_4/TNT increases with the increase of Ag_3PO_4 content. When the $AgNO_3$ concentration exceeds 60 mmol L^{-1}, the photocatalytic activity of Ag_3PO_4/TNT begins to decline. This phenomenon can be attributed to the balance between the content of Ag_3PO_4 crystal on the TNT surface and the exposed reactive sites. With the increase of $AgNO_3$ mass ratio, Ag_3PO_4/TNT has higher photo−absorption capability for visible light and renders more reactive sites, thus possessing higher photocatalytic activity. However, as the $AgNO_3$ concentration is higher than 60 mmol L^{-1}, Ag_3PO_4 nanoparticles become large and tend to aggregate on the TNT surface (Fig. S3), thereby lowering the exposed reactive sites and photocatalytic activity. The kinetic curves for the RhB degradation over all photocatalysts are plotted, and illustrated in Fig. 6b. All of them fit well with the pseudo−first order correlation, $\ln (C_0/C) = kt$, where k is the apparent reaction rate constant, C_0 and C are the initial and instantaneous concentrations of RhB, respectively. The k value of Ag_3PO_4/TNT−60 is 0.234 min^{-1}, which is about 8.7 times of that of pure Ag_3PO_4.

The adsorption of organic molecules to the catalyst surface is a pivotal step for photocatalytic degradation. [30] As shown in Fig. 6a, after adsorption equilibrium in the dark for 1 h, 8.2% of RhB molecules are adsorbed with Ag_3PO_4 as the catalyst; while more RhB molecules (ca. 19.7%) are adsorbed on the surface of Ag_3PO_4/TNT photocatalysts. This result can be ascribed to high specific surface area of TNT (287.8 m^2 g^{-1}) and the small size of Ag_3PO_4 nanocrystals. Besides, the uniform growth of Ag_3PO_4 nanoparticles on the dispersive TNT makes a sufficient utilization of visible light, which is superior to that of Ag_3PO_4/TiO_2 nanotube array composites where Ag_3PO_4 deposited on the void and/or the top of TiO_2 nanotube arrays. [7, 20] It is believed that the enhanced adsorption capacity, abundant active sites and sufficient light absorbance facilitate the photocatalytic degradation performance of Ag_3PO_4/TNT for organic dyes.

Photocatalytic mechanism

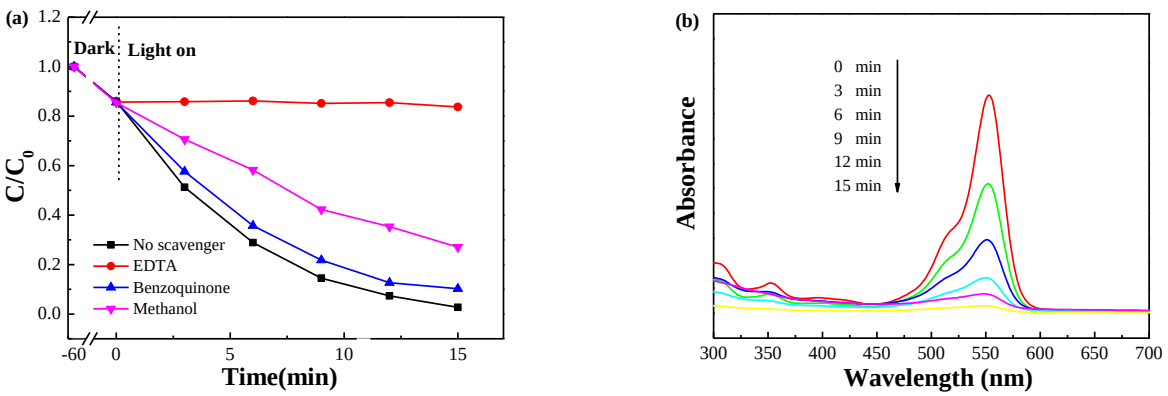

Fig. 7 (a) Visible−light photocatalytic degradation of RhB in the presence of EDTA, benzoquinone and methanol over Ag_3PO_4/TNT−20; (b) UV−vis spectrum change of RhB during photocatalytic process over Ag_3PO_4/TNT−20.

To further reveal the photocatalytic mechanism, EDTA, methanol and benzoquinone were employed as the scavengers of h^+, ·OH, and $\cdot O_2^-$ to investigate the specific reactive species involved in the RhB degradation over Ag_3PO_4/TNT−20, respectively. [8] As illustrated in Fig. 7a, the RhB degradation is remarkably suppressed with the addition of EDTA, which only has a degradation efficiency of 2% within 15 min irradiation. This result indicates that h^+ is the dominant active specie in the degradation of RhB by Ag_3PO_4/TNT. The methanol can partly suppress the RhB degradation throughout the reaction, suggesting that ·OH radicals also play an important role in the photocatalytic reaction. The effect of ·OH radicals can be further confirmed with the UV−vis spectrum change of RhB during the photocatalytic process. As can be seen from Fig. 7b, the maximum absorption of RhB catalyzed by Ag_3PO_4/TNT−20 retains at 553 nm without any blue shift during the reaction. It is well accepted that the photocatalytic degradation of RhB proceeds *via* two competitive processes, the N−de−ethylation process and the destruction of the conjugated structure. [27, 31] The former can produce the intermediates with different numbers of N−ethyl groups, which are removed sequentially from the parent RhB molecules, leading to the absorption peak of RhB blue shift; while the latter can generate *N*,*N*−diethyl−*N*'−ethylrhodamine (DER), *N*−ethyl−*N*'−ethyl−rhodamine (EER), *N*,*N*−diethyl−rhodamine (DR) and some organic acids deriving from the cleavage of the xanthene ring in the RhB structure, which results in the rapid decrease of RhB absorption peak, but no new peak appearing. [31] Therefore, h^+ and ·OH radicals degrade RhB through the destruction of the conjugated structure during the photocatalytic process by Ag_3PO_4/TNT. [27] The detail process is deduced as follows: the Ag_3PO_4/TNT photocatalyst has high adsorption capacity for RhB molecules, leading to direct h^+ oxidation of RhB on its surface. Meanwhile, some h^+ can also react with water to generate ·OH radicals, which subsequently decompose RhB molecules. Accordingly, both h^+ and ·OH radicals in solution make some contribution to the photocatalytic reaction. Moreover, Fig. 7a demonstrates that the RhB degradation is hardly suppressed by benzoquinone, indicating that

$\cdot O^{2-}$ is not one of the main active radicals during the photocatalytic process. The CB of Ag_3PO_4 is +0.45 eV, which is higher than the reduction potential of $\cdot O^{2-}/O_2$ (−0.33 eV), thus the photo−generated electrons cannot reduce O_2 to $\cdot O^{2-}$. [1] It has been reported that the photo−generated electrons can react with H^+ and O_2 to produce H_2O_2 ($O_2 + 2H^+ + 2e^- = H_2O_2$, +0.695 eV), which is advantageous for photocatalysis. [3, 12, 32]

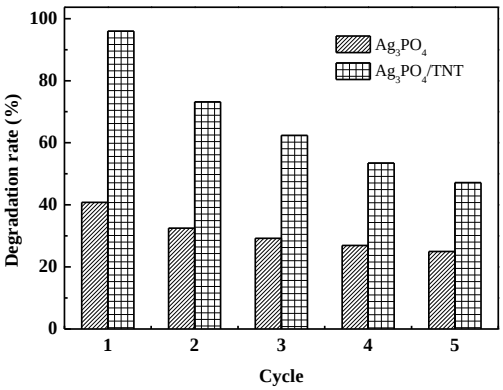

Fig. 8 Five cycles of the RhB degradation photocatalyzed by Ag_3PO_4/TNT−20 under visible light.

To further investigate the operation stability of Ag_3PO_4/TNT photocatalyst, herein, the used Ag_3PO_4/TNT powder was collected just by centrifugation, and reused in five successive RhB degradation experiments. As shown in Fig. 8, although some photocatalytic activity losses are observed for Ag_3PO_4/TNT photocatalyst in five experimental runs, the activity is still better than that of the fresh pure Ag_3PO_4, which is not observed in some other Ag_3PO_4−semicondutor composites. [8, 33–34] This relatively remarkable performance of the heterojunction is attributed to its more reaction sites. Hence, Ag_3PO_4/TNT heterojunction appears to be more desirable in the repeated and/or long−term application, which exhibits high photocatalytic activity after recycling. [12] The inevitable loss of photocatalytic activity may be assigned to the small size of Ag_3PO_4 nanoparticles, which tends to be easily reduced into Ag. As can be seen from Fig. S1, the characteristic peak of Ag nanoparticles ($2\theta=37.8^o$) [3] appears after reused in three degradation experiments. With appropriate Ag nanoparticles, a sandwiched Ag/Ag_3PO_4/TNT heterostructure can promote the charge separation, and the further reduction of Ag_3PO_4 could be inhibited by injecting photo−generated electrons into the conduction band of TNT through the Ag/TNT interface. [3, 12, 28]

On the basis of the above experimental results and the previous reports, [12, 24] it is deduced that the unusual high catalytic efficiency of the Ag_3PO_4/TNT photocatalyst originates from the band match between these two semiconductors. The photocatalytic mechanism is proposed in Scheme 2. Under visible−light irradiation, the photo−generated electrons are excited from valence band (VB) to conduction band (CB) in Ag_3PO_4, inducing the formation of holes in the VB simultaneously. The photo−generated holes in the VB of Ag_3PO_4 can quickly transfer to the TNT surface, since the VB potential of Ag_3PO_4 (+2.9 eV) is more positive than that of TiO_2 (+2.7 eV). [12, 24] Consequently, the heterojunction significantly accelerates the charge carrier transfer between two semiconductors, which enables the efficient separation of photo−generated electron−hole pairs from Ag_3PO_4. As a result, both the holes transferring to the VB of TNT and remaining in the VB of Ag_3PO_4 can be employed for the subsequent oxidation reactions of RhB. Some Ag nanoparticles may generate by self-reduction during irradiation process (Fig. S1 and S2), which can trap the photo−generated electrons, thus facilitating the electron-hole separation and improving the photocatalytic activity.

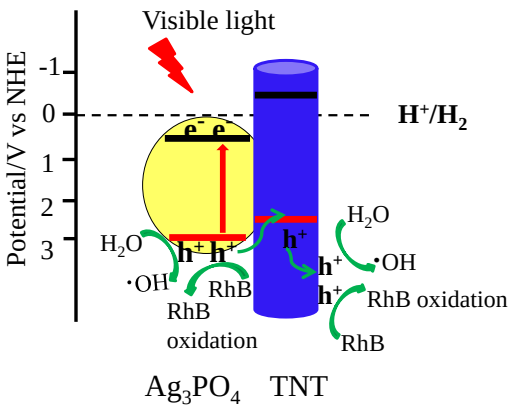

Scheme 2 Schematic illustration of photocatalytic degradation mechanism of RhB over Ag_3PO_4/TNT heterojunctions under visible light.

Conclusion

In summary, the Ag_3PO_4/TNT heterojunction has been successfully fabricated *via* a facile *in situ* method, in which Ag_3PO_4 crystals about several nanometers in size are homogeneously grown on the TNT surface. The TNT not only accelerates the separation of photo−generated electron−hole pairs, but also enhances the dye adsorption capacity, thereby significantly improving the photocatalytic activity of Ag_3PO_4/TNT under visible light irradiation. TNT moiety in the heterojunction rendered an intensified light absorption, because the band gaps of Ag_3PO_4/TNT samples originated from TNT moiety are much narrower than that of pure TNT. During the photocatalytic process, h^+ plays a critical role, which can directly oxidize RhB molecules or produce ·OH radicals that further degrade RhB molecules through the destruction of the conjugated structure. Meanwhile, the Ag_3PO_4/TNT heterojunction preserves high photocatalytic activity after used for five cycle reactions.

Acknowledgements

This work is supported by National Science Fund for Distinguished Young Scholars (21125627) and the Program of Introducing Talents of Discipline to Universities (No. B06006).

Notes and references

[a] *Key Laboratory for Green Technology, School of Chemical Engineering and Technology, Tianjin University, Tianjin 300072, China*
[b] *Key Laboratory of Systems Bioengineering of Ministry of Education, School of Chemical Engineering and Technology, Tianjin University, Tianjin 30072, China*
[c] *School of Environmental Science and Engineering, Tianjin University, 300072 Tianjin, China*
[d] *Collaborative Innovation Center of Chemical Science and Engineering (Tianjin), Tianjin 300072, China*

Electronic Supplementary Information (ESI) available: [details of any supplementary information available should be included here]. See DOI: 10.1039/b000000x/

1 Z. G. Yi, J. H. Ye, N. Kikugawa, T. Kako, S. Ouyang, H. Stuart−Williams, H. Yang, J. Y. Cao, W. J. Luo, Z. S. Li, Y. Liu and R. L. Withers, *Nat. Mater.* 2010, ***9***, 559.
2 Y. P. Bi, S. X. Ouyang, N. Umezawa, J. Y. Cao and J. H. Ye, *J Am. Chem. Soc*. 2011, ***133***, 6490.
3 J. J. Guo, S. X. Ouyang, P. Li, Y. J. Zhang, T. Kako and J. H. Ye, *Appl. Catal. B Environ*. 2013, ***134−135,*** 286.
4 H. C. Zhang, H. Huang, H. Ming, H. T. Li, L. L. Zhang, Y. Liu and Z. H. Kang, *J. Mater. Chem*. 2012, ***22,*** 10501.
5 X. F. Yang, H. Y. Cui, Y. Li, J. L. Qin, R. X. Zhang and H. Tang, *ACS Catal*. 2013, ***3***, 363.
6 W. C. Peng, X. Wang and X. Y. Li, *Nanoscale* 2014, ***6***, 8311.
7 W. Teng, X. Y. Li, Q. D. Zhao and G. H. Chen, *J. Mater. Chem. A* 2013, ***1***, 9060−9068.
8 Z. H. Chen, W. L. Wang, Z. G. Zhang and X. M. Fang, *J. Phys. Chem. C* 2013, ***117***, 19346.
9 H. Katsumata, T. Sakai, T. Suzuki and S. Kaneco, *Ind. Eng. Chem. Res*. 2014, ***53***, 8018.
10 Y. P. Bi, H. Y. Hu, S. X. Ouyang, Z. B. Jiao, G. X. Lu and J. H. Ye, *J. Mater. Chem.* 2012, ***22***, 14847.
11 Y. P. Liu, L. Fang, H. D. Lu, Y. W. Li, C. Z. Hu and H G. Yu, *Appl. Catal. B Environ*. 2012, ***115***, 245.
12 W. F. Yao, B. Zhang, C. P. Huang, C. Ma, X. L. Song and Q. J. Xu, *J. Mater. Chem.* 2012, ***22***, 4050.
13 C. Ratanatawanate, C. R. Xiong and K. J. Balkus Jr, *ACS nano* 2008, ***2***, 1682.
14 Z. R. Tang, Y. Zhang and Y. J. Xu, *ACS Appl. Mater. Interfaces* 2012, ***4***, 1512.
15 K. Kiatkittipong, J. Scott and R. Amal, *ACS Appl. Mater. Interfaces* 2011, ***3***, 3988.
16 J. Y. Kim, J. H. Noh, K. Zhu, A. F. Halverson, N. R. Neale, S. Park, K. S. Hong and A. J. Frank, *ACS Nano* 2011, ***5***, 2647.
17 R. M. Navarro, M. C. Alvarez−Galvan, J. A. Villoria de la Mano, S. M. Al−Zahrani and J. L. G. Fierro, *Energy Environ. Sci*. 2010, ***3***, 1865.
18 B. K. Vijayan, N. M. Dimitrijevic, D. Finkelstein−Shapiro, J. S. Wu and K. A. Gray, *ACS Catal*. 2012, ***2***, 223.
19 N. K. Shrestha, J. M. Macak, F. Schmidt−Stein, R. Hahn, C. T. Mierke, B. Fabry and P. Schmuki, *Angew. Chem. Int. Ed.*. 2009, ***48***, 969.
20 M. Niraula, S. Adhikari, D. Y. Lee, E. K. Kim, S. J. Yoon, S. K. Dhungel, W. Lee, N. K. Shrestha and S. H. Han, *Chem. Phys. Lett*. 2014, ***593***, 193.
21 J. Q. Geng, Z. Y. Hang, Y. Wang and D. Yang, *Scripta Mater*. 2008, ***59***, 352.
22 Z. M. Yang, G. F. Huang, W. Q. Huang, J. M. Wei, X. G. Yan, Y. Y. Liu, C. Jiao, Z. Wan and A. Pan, *J. Mater. Chem. A* 2014, ***2***, 1750.
23 Y. C. Liang, C. C. Wang, C. C. Kei, Y. C. Hsueh, W. H. Cho and T. P. Perng, *J. Phys. Chem. C* 2011, ***115***, 9498.
24 X. F. Yang, J. L. Qin, Y. Jiang, R. Li, Y. Li and H. Tang, *RSC Advances* 2014, ***4***, 18627.
25 Q. H. Liang, Y. Shi, W. J. Ma, Z. Li and X. M. Yang, *Phys Chem Chem Phys* 2012, ***14***, 15657.
26 Y. Y. Wen, H. M. Ding and Y. K. Shan, *Nanoscale* 2011, ***3***, 4411.
27 C. Liu, D. Yang, Y. Jiao, Y. Tian, Y. G. Wang and Z. Y. Jiang, *ACS Appl. Mater. Interfaces* 2013, ***5***, 3824.
28 Y. P. Bi, S. Ouyang, J. Y. Cao and J. H. Ye, *Phys Chem Chem Phys* 2011, ***13***, 10071.
29 H. H. Li, S. Yin, Y. H. Wang, T. Sekino, S. W. Lee and T. Sato, *J. Mater. Chem. A* 2013, ***1***, 1123.
30 J. Du, X. Y. Lai, N. L. Yang, J. Zhai, D. Kisailus, F. B. Su, D. Wang and L. Jiang, *ACS nano* 2010, ***5***, 590.
31 C. C. Chen, W. Zhao, J. Y. Li, J. C. Zhao, H. Hidaka and N. Serpone, *Environ. Sci. Technol*. 2002, ***36***, 3604.
32 S. B. Rawal, S. D.Sung and W. I. Lee, *Catal. Commun.* 2012, ***17***, 131.
33 Y. S. Xu and W. D. Zhang, *Dalton Trans*. 2013, ***42***, 1094.
34 R. Y. Liu, P. G. Hu and S. W. Chen, *Appl. Surf. Sci*. 2012, ***258***, 9805.